JOURNAL OF GEOPHYSICAL RESEARCH, VOL. 91, NO. B6, PAGES 6405–6417, MAY 10, 1986

Thermal Stress and the Spacings of Transform Faults

DAVID T. SANDWELL

Institute for Geophysics, University of Texas at Austin

Bathymetric charts are used with satellite altimeter profiles to locate major ridge-transform intersections along five spreading ridges. The ridges are the Mid-Atlantic Ridge, the East Pacific Rise, the Chile Rise, the Pacific-Antarctic Rise, and the Southeast Indian Ridge. Analysis of these data show spacings between transform faults W increase linearly with spreading rate v (W/v = 6.28 m.y.). This linear correlation is explained by a thermoelastic model of a cooling strip of lithosphere spreading at a rate v. The traction-free boundaries of the thin elastic strip simulate cracks in the lithosphere at transform faults. A two-dimensional thermoelastic solution for the in-plane stress shows the largest stress component is tensional and parallel to the ridge. Stresses are zero at the ridge and increase as (age)$^{1/2}$ to a maximum value at an age of $W/4v$. All stress components are small for ages greater than W/v. When the transform spacing is large compared with the spreading rate (W/v > 100 m.y.) thermal stresses exceed the strength of the lithosphere for ages between 0 and 30 Ma. The observed maximum ratio of transform spacing to spreading rate (W/v = 10 m.y.) results in low thermal stresses that only exceed the strength of the lithosphere for ages less than 1 Ma. Thus transform faults relieve most of the thermal stress. Model predictions also agree with earthquake studies showing that normal faults in young lithosphere have tensional axes aligned with the ridge. Moreover, oceanic intraplate earthquakes rarely occur in lithosphere older than 30 Ma as predicted by the model. These and other geophysical observations confirm *Turcotte*'s hypothesis that transform faults are thermal contraction cracks.

Introduction

The orthogonal pattern of ridges and transform faults along oceanic spreading ridges preserves the initially jagged tear of continental lithosphere [*Wilson*, 1965]. The most notable example is the Mid-Atlantic Ridge which closely reflects the continental margins of Africa and the Americas. The curving Mid-Atlantic Ridge is actually composed of short, straight ridge and transform segments. According to plate tectonic theory, the transform segments must be parallel to the spreading direction. The spreading ridge segments are usually perpendicular to the spreading direction [*Atwater and Macdonald*, 1977]. This ridge orthogonality is not required by plate tectonic theory but is believed to be a consequence of spreading dynamics [*Lachenbruch*, 1973; *Froidevaux*, 1973; *Oldenburg and Brune*, 1975; *Stein*, 1978]. Two basic types of spreading boundaries can be constructed from orthogonal ridges and transforms. The stepped pattern, shown in Figure 1*a*, results in an average plate boundary (dashed line) that is oblique to the spreading direction. The crenelate pattern, shown in Figure 1*b*, results in an average plate boundary (dashed line) that is nearly orthogonal to the spreading direction [*Menard*, 1984]. (Stepped and crenelate are called type I and type II, respectively, by *Turcotte* [1974].) Left-lateral and right-lateral stepped patterns connected by a crenelate pattern can be combined to produce a curved spreading boundary. Thus it appears that the observed orthogonality of ridges to the spreading direction and the curvature of the plate boundary, reflecting continental breakup, explain the existence of transform faults.

Despite this simple explanation, there are at least three lines of observational evidence indicating that transform faults are an inherent part of the spreading process and are not just required for oblique spreading. First bathymetric charts [*Chase et al.*, 1970], magnetic lineation maps [*Atwater and Menard*, 1970; *Vogt and Cherkis*, 1983], and satellite altimeter data presented below show cases where crenelate patterns are connected to crenelate patterns. These combinations of ridge segments and transforms could evolve to a single straight ridge. However, the opposite development is known to occur. For example, south of the Mendocino fracture zone, in the late Cretaceous, a crenelate pattern developed from an initially long straight segment of spreading ridge [*Winterer*, 1976]. *Menard* [1984] describes how this crenelate pattern developed through asymmetrical spreading, but his model does not explain why this complicated pattern developed. Crenelate patterns along other spreading ridge boundaries could degenerate to long straight ridge segments, but they do not.

The second line of evidence is the existence of zero offset fracture zones discovered by *Schouten and White* [1980]. Indeed their detailed magnetic anomaly map of the seafloor southwest of Bermuda shows a left-lateral transform fault that shortened to zero length and emerged along the same part of the ridge as a right-lateral transform. The fact that it emerged in the same spot indicates that either the stress field of the lithosphere or the convection patterns beneath the ridge determine the location of the transform fault. *Schouten and Klitgord* [1982] prefer the latter model.

The final line of evidence that transform faults are an inherent part of the spreading process is the correlation between ridge segment length and spreading rate [*Fox and Gallo*, 1984]. To quantify this relationship, ridge-transform intersection locations are derived from satellite altimeter data and bathymetry data. Using this digital plate boundary, along with the *Minster and Jordan* [1978] present-day spreading model, a linear relationship between ridge segment length and spreading rate is found. Any model for the existence of transform faults must reproduce this linear rate dependence.

Paper number 5B5674.
0148-0227/86/005B-5674$05.00

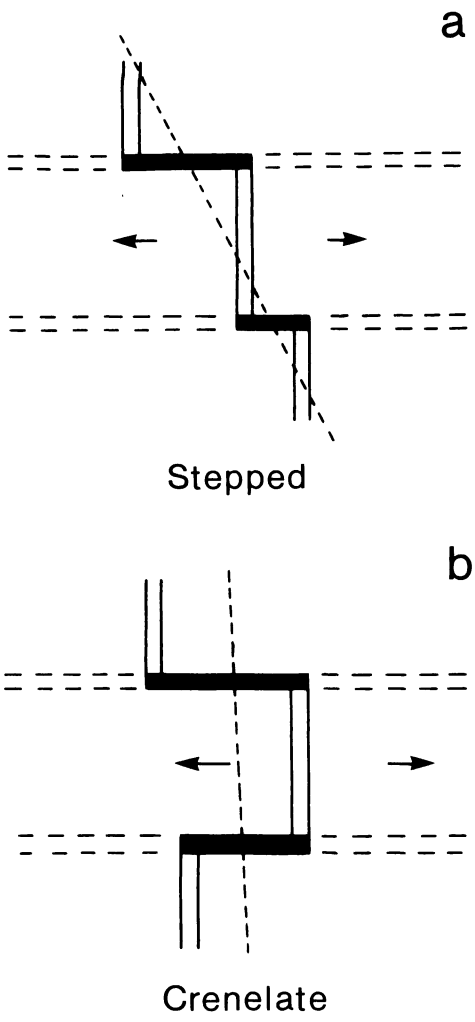

Fig. 1. Types of orthogonal ridge and transform patterns. *(a)* Stepped pattern, *(b)* Crenelate pattern.

Several models for the orthogonal ridge-transform pattern have been proposed. The initial theory that the pattern preserves the jagged continental rift has both observational [*Wilson*, 1965] and experimental justification. The wax models of *Oldenburg and Brune* [1972, 1975] were used to derive the necessary conditions for development and maintenance of the orthogonal pattern. These conditions are as follows: (1) the applied stress field must be symmetric, (2) the film of solid material over the ridge crest must fracture in a brittle manner, and (3) the shear strength of the material must exceed the shear stress on the transform fault. This last criterion explains the disintegration of the ridge-transform pattern along the fastest spreading portions of the East Pacific Rise [*Fox and Gallo*, 1984]. The wax models exhibit much of the observed anomalous behavior described above including the crenelate pattern and its development from asymmetrical spreading. Zero offset fracture zones and the relationship between ridge segment length and spreading rate were not reported in the wax experiments, although they may occur. The wax models reveal the dynamics of the orthogonal pattern, but they do not explain why it occurs.

A model for ridge segmentation was proposed by *Schouten and Klitgord* [1982] based on their observation of zero offset fracture zones. They suggest that stationary convection cells independently influence the accretion process. Each cell is bounded by fracture zones, and its episodic intrusion process will usually be out of phase with the adjacent cells. This independence provides a memory mechanism for times when a transform fault has zero offset. More recently, *Dick et al.* [1984] proposed that a cylinder of partially molten material beneath the ridge becomes gravitationally unstable resulting in a segmented ridge. These convection type models can be adjusted to explain all of the observations but fail to consider the properties or response of the lithosphere.

Turcotte [1974] proposed that transform faults are thermal contraction cracks. He used a simple plane strain approximation to calculate the along-ridge tensile stress that develops as the lithosphere ages, cools, and contracts. His calculations show that thermal stresses exceed the strength of the upper brittle lithosphere. The cracks develop as transform faults. His model is in accordance with the depth versus age results [*Parsons and Sclater*, 1977] which show the lithosphere shrinks in all three dimensions by as much as 1%. Recent estimates of lithospheric strength, derived from experimental rock mechanics [*Goetze and Evans*, 1979], indicate the entire lithosphere should fail under the thermal stress. Therefore *Turcotte*'s simple model which agrees with established properties of the lithosphere explains the existence of transform faults; they relieve thermal stress. The only observation not explained by his model is the linear relationship between ridge segment length and spreading rate.

In this study it is shown that a more elaborate thermoelastic model also predicts the linear relation between velocity and ridge segment length. The lithosphere is modelled as a thin rectangular plate (plane stress approximation) with the temperature structure of a cooling half-space. Three of the plate's edges are traction free, while the fourth edge, corresponding to the spreading ridge, also has zero shear stress. This simulates freezing of material at the ridge. Model calculations show that the amplitude of the thermal stress is proportional to the ridge segment length and inversely proportional to the spreading rate. Thus constant maximum stress is attained if ridge segment length is proportional to spreading rate. The model also predicts that the zone of high stress is confined to a distance of one half ridge segment length from the ridge. This latter prediction is in agreement with earthquake studies showing the rapid decline in earthquake frequency as the lithosphere ages [*Wiens and Stein*, 1983,1984; *Bergman and Solomon*, 1984]. Most near-ridge earthquakes are normal faults with their tensional axis aligned with the spreading ridge. Several investigators [*Bratt et al.*, 1985; *Bergman and Solomon*, 1984] have recently explained these earthquake characteristics in terms of thermal stress.

Data Analysis

Two types of data were used to locate intersections between ridge segments and transform faults. In areas of adequate bathymetric coverage, such as the North Atlantic and North Pacific, ridge-transform intersections were digitized from the GEBCO map series [*Canadian Hydrographic Service*, 1982]. In more remote areas, where

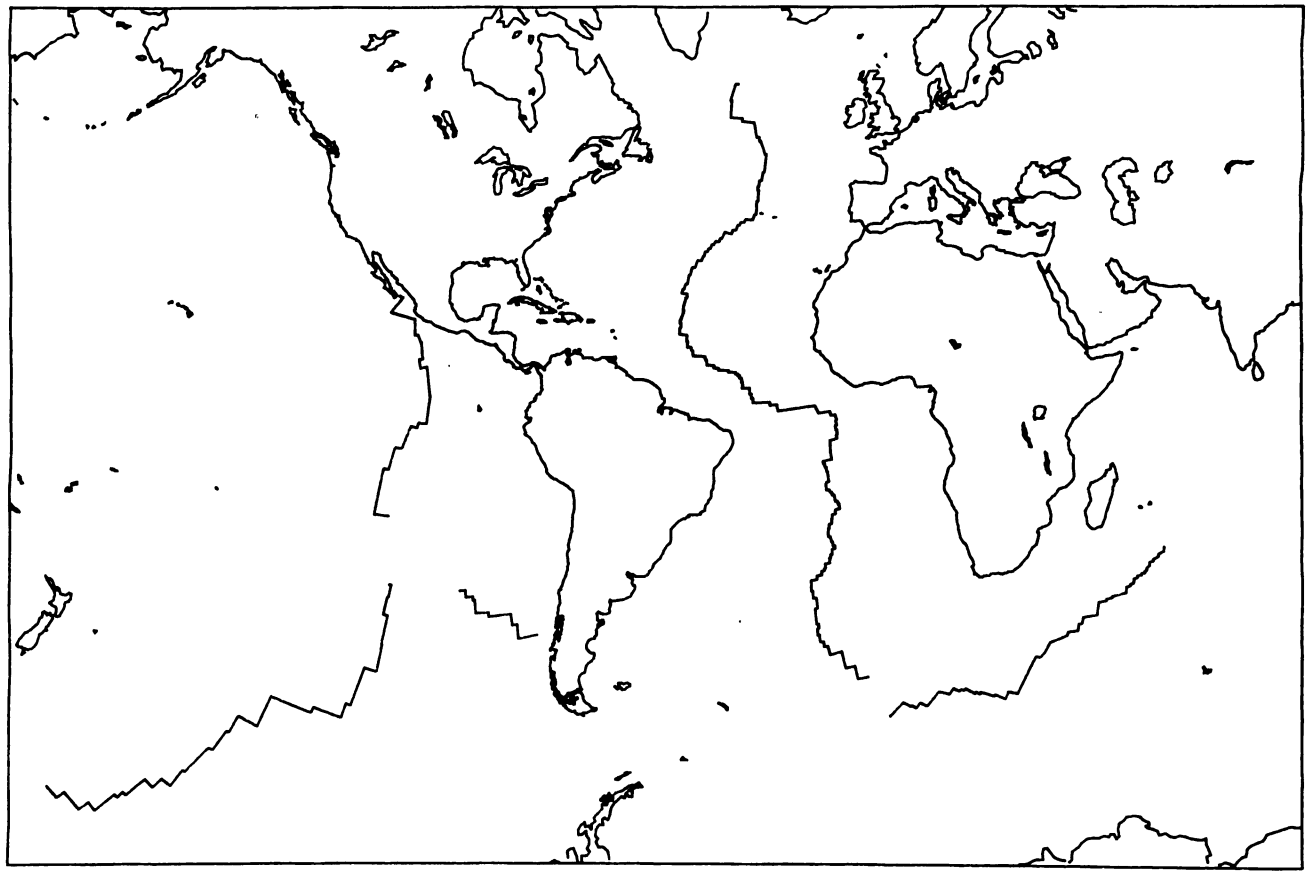

Fig. 2. Spreading ridge boundaries derived from bathymetry and satellite altimeter data.

the transform faults are not properly charted, Seasat and GEOS 3 altimeter data were used to define the trends of the fracture zones (FZs). This is possible because FZs, with offsets greater than a few million years, produce characteristic signals that correlate among many altimeter passes [*Crough*, 1979; *Detrick*, 1981; *Sandwell*, 1984]. The overall trends of the ridges are apparent on the bathymetric charts. Slow spreading ridges are also apparent in the altimeter profiles because geoid height decreases linearly with age [*Haxby and Turcotte*, 1978]. If it is assumed that each ridge segment is perpendicular to the FZ, then even in poorly charted areas, ridge-transform intersections can be approximately located. Spreading ridges showing no clear orthogonal ridge-transform pattern (e.g., south of Australia) were not analyzed.

In areas of sparse bathymetric coverage the locations of ridge-transform intersections may be in error. However, the exact locations are not important for determining characteristic ridge segment length. Instead it is important that significant transform faults are not omitted, since an omission doubles the length of the ridge segment. Most small-age-offset transform faults and other minor interruptions of a spreading ridge will not be found with this technique. This is because minor interruptions do not appear on the GEBCO charts which were produced from single-beam bathymetric profiles. Detailed maps of selected areas, produced from multibeam bathymetric data, show that ridge interruptions occur every 30 km along slow spreading ridges and every 70 km along fast spreading ridges (*D. Abbott*, unpublished manuscript, 1985). Major ridge interruptions (i.e., transform faults with age offset > 2 m.y.) occur much less frequently. It is shown below that only significant-age-offset transform faults relieve thermal stress. The data presented here reflect these significant offsets.

Five continuous ridge boundaries were digitized by this technique. They are the Mid-Atlantic Ridge, the East Pacific Rise, the Chile Rise, the Pacific-Antarctic Rise, and the Southeast Indian Ridge. These plate boundaries are shown in Figure 2, and the ridge-transform locations are given in Table 1. The two geographic positions in each row of the table are the end points of each transform fault. The following two integers indicate the plates on the left and right sides of the boundary, respectively [*Minster and Jordan*, 1978]. The named FZs are also listed in Table 1. Note the congruence of the Mid-Atlantic Ridge and the continental margins (and even the coastlines) of Africa and the Americas. This close correspondence favors the original explanation for the existence of transform faults; they are required for oblique spreading [*Wilson*, 1965]. Note, however, the difference in characteristic ridge segment length between the Mid-Atlantic Ridge and the East Pacific Rise. Since the East Pacific Rise spreads about 5 times faster than the Mid-Atlantic Ridge, it appears that ridge length is associated with spreading rate.

Using the data presented in Table 1, along with the present-day plate motion model of *Minster and Jordan* [1978], one can examine various relationships among ridge segment length, transform length, spreading rate, and the

TABLE 1. Ridge-Transform Intersections

Latitude	Longitude	Latitude	Longitude	Plate* L	Plate* R	Fracture Zone
		Mid Atlantic Ridge				
57.00	326.40	57.00	325.80	9	6	Bight
55.00	324.70	55.00	325.00	9	6	
52.80	324.75	52.70	327.35	9	6	Charlie Gibbs
52.30	327.35	52.15	330.00	9	6	Charlie Gibbs
50.20	330.50	50.20	331.05	9	6	Faraday
49.65	331.10	49.60	331.40	9	6	Faraday
47.80	332.30	47.80	332.60	9	6	Maxwell
45.10	332.20	45.10	331.90	9	6	
43.80	331.60	43.82	331.10	9	6	
42.90	331.00	42.90	330.75	9	6	
42.30	330.70	42.30	330.95	9	6	
40.50	330.80	40.50	330.50	9	6	
38.30	330.40	38.30	330.05	9	1	
37.40	329.70	37.55	328.10	9	1	Pico
36.95	327.75	37.00	327.00	9	1	
36.50	326.75	36.52	326.35	9	1	
35.58	325.90	35.62	325.20	9	1	
34.97	325.00	35.30	323.50	9	1	Oceanographer
34.10	322.80	34.15	322.40	9	1	
33.50	322.20	33.65	321.40	9	1	Hayes
32.95	321.00	33.05	320.60	9	1	
32.28	320.30	32.30	319.90	9	1	
31.70	319.60	31.72	319.10	9	1	
30.89	318.90	30.90	318.70	9	1	
30.00	318.30	30.10	317.40	9	1	Atlantis
28.75	316.85	28.75	316.25	9	1	
27.25	315.75	27.27	315.50	9	1	
25.50	315.10	25.60	314.70	9	1	
24.55	314.40	24.60	314.10	9	1	
23.75	313.80	23.60	315.10	9	1	Kane
22.85	315.10	22.90	314.70	9	1	
22.00	314.60	22.00	314.45	9	1	
21.30	314.40	21.30	314.25	9	1	
20.30	314.15	20.30	314.40	9	1	
19.80	314.30	19.80	314.10	9	1	
19.00	314.00	19.00	313.80	9	1	
18.45	313.80	18.45	313.50	9	1	
17.70	313.45	17.65	313.75	9	1	
16.75	313.70	16.75	313.45	9	1	
15.40	313.40	15.20	315.10	11	1	Fifteen-Twenty
13.95	314.95	13.90	315.25	11	1	
12.70	315.10	12.65	316.00	11	1	
12.05	316.00	12.00	316.40	11	1	
10.90	316.35	10.70	319.10	11	1	Vema
10.02	319.10	10.00	319.40	11	1	
8.90	319.50	8.80	321.05	11	1	
8.25	321.00	8.25	322.05	11	1	
7.80	322.05	7.75	324.30	11	1	Doldrums
7.40	324.35	7.40	325.85	11	1	
7.00	325.90	7.00	326.40	11	1	
6.70	326.40	6.70	326.75	11	1	
6.15	326.75	6.15	327.20	11	1	Sierra Leone
5.40	327.10	5.40	327.40	11	1	
4.70	327.35	4.70	327.50	11	1	
3.95	327.25	4.00	329.00	11	1	Four North
2.70	329.01	2.70	329.40	11	1	
1.75	329.40	1.75	329.75	11	1	
0.80	329.75	0.95	333.50	11	1	
0.25	333.55	0.40	335.10	11	1	St. Paul
-1.00	335.30	0.25	343.50	11	1	Romanche
-1.40	344.25	-1.00	346.75	11	1	Chain
-1.90	347.00	-1.70	347.90	11	1	
-2.85	348.20	-3.00	347.95	11	1	
-4.05	348.20	-4.15	347.90	11	1	
-5.10	347.95	-5.10	348.20	11	1	
-6.10	348.30	-6.20	348.10	11	1	
-7.00	348.20	-7.35	346.65	11	1	Ascension
-8.50	346.80	-8.55	346.70	11	1	
-9.70	346.80	-9.75	346.75	11	1	
-11.50	347.10	-11.90	345.10	11	1	

TABLE 1. (continued)

Latitude	Longitude	Latitude	Longitude	Plate* L	Plate* R	Fracture Zone
-12.40	345.25	-12.35	345.50	11	1	
-13.15	345.65	-13.10	345.90	11	1	
-14.10	346.00	-14.10	346.15	11	1	
-14.80	346.25	-14.80	346.25	11	1	
-16.25	346.45	-16.40	345.70	11	1	
-17.95	345.90	-17.80	346.50	11	1	St. Helena
-18.35	346.65	-18.30	347.05	11	1	
-18.90	347.10	-18.85	347.55	11	1	Hotspur
-20.20	347.80	-20.15	348.30	11	1	Martin Vaz
-20.75	348.35	-20.70	348.60	11	1	
-21.75	348.75	-21.95	347.75	11	1	
-22.80	347.80	-22.95	347.05	11	1	
-23.80	347.10	-23.85	346.95	11	1	
-24.75	347.00	-24.85	346.40	11	1	
-25.70	346.50	-25.70	346.25	11	1	
-26.80	346.25	-26.80	346.25	11	1	
-27.25	346.30	-27.20	346.75	11	1	
-28.25	346.95	-28.25	347.20	11	1	
-29.00	347.30	-29.00	347.75	11	1	Rio Grande
-29.60	347.80	-29.70	347.10	11	1	
-30.70	347.15	-30.75	346.80	11	1	
-31.40	346.75	-31.40	346.55	11	1	
-32.30	346.60	-32.45	345.60	11	1	
-33.30	345.65	-33.35	345.40	11	1	
-33.70	345.40	-33.80	344.80	11	1	
-34.50	344.80	-34.65	343.75	11	1	
-35.35	343.80	-35.45	342.50	11	1	
-37.30	342.60	-37.30	342.90	11	1	Tristan Da Cunha
-38.50	343.00	-38.40	343.70	11	1	
-40.20	343.95	-40.30	343.40	11	1	Gough
-42.75	343.75	-42.70	344.20	11	1	
-43.45	344.30	-43.50	343.90	11	1	
-44.45	344.00	-44.40	344.40	11	1	
-45.50	344.50	-45.45	345.30	11	1	
-46.20	345.40	-46.10	346.20	11	1	
-47.40	346.70	-46.90	349.25	11	1	Agulhas
-49.30	350.10	-49.00	352.10	11	1	
-50.80	352.75	-50.50	355.05	11	1	
		East Pacific Rise				
23.20	251.25	22.90	251.95	10	5	Tamayo
19.90	249.20	18.45	254.60	10	5	Rivera
15.20	254.65	15.25	255.30	10	5	Orozco
13.70	255.90	13.70	256.05	10	5	O'Gorman
10.10	256.30	10.10	255.50	10	5	Clipperton
8.20	255.80	8.55	257.20	10	5	Siqueiros
2.20	257.90	2.20	257.95	10	5	Colon Ridge
-3.80	257.10	-3.50	255.40	10	8	Quebrada
-4.70	255.05	-4.30	253.70	10	8	Gofar
-9.20	251.70	-8.90	250.20	10	8	Wilkes
-13.65	248.85	-13.40	247.75	10	8	Garrett
-22.95	245.55	-23.30	248.75	10	8	
		Chile Rise				
-37.25	264.50	-37.20	265.70	2	8	Chile
-38.40	265.75	-38.30	267.35	2	8	
-38.95	267.35	-38.90	267.75	2	8	
-41.05	268.00	-40.95	270.80	2	8	
-41.65	270.90	-41.15	275.80	2	8	Valdivia
-43.00	276.15	-42.85	277.20	2	8	
-45.05	277.50	-44.45	281.65	2	8	Guafo
		Pacific-Antarctic Rise				
-36.25	249.00	-36.30	249.40	10	2	
-38.40	248.75	-38.40	248.50	10	2	
-41.25	247.60	-41.50	248.60	10	2	
-46.00	247.25	-46.05	247.35	10	2	
-49.85	246.20	-49.30	243.50	10	2	Menard
-54.30	240.50	-54.05	239.50	10	2	
-55.85	238.40	-54.50	232.25	10	2	Heezen
-55.20	231.70	-53.15	222.75	10	2	Tharp
-56.90	219.60	-55.60	215.40	10	2	Udintsev
-57.60	213.25	-57.45	212.70	10	2	
-59.60	209.65	-59.40	208.70	10	2	

TABLE 1. (continued)

Latitude	Longitude	Latitude	Longitude	Plate* L	Plate* R	Fracture Zone
-61.90	203.60	-61.75	203.00	10	2	
-63.30	200.40	-62.60	198.50	10	2	
-63.45	196.50	-62.65	194.80	10	2	
-64.20	190.60	-63.90	189.90	10	2	
-64.40	188.80	-64.15	188.05	10	2	
-65.60	183.80	-64.85	182.40	10	2	
-65.50	180.30	-63.90	177.10	10	2	
-64.45	175.50	-63.30	173.25	10	2	Scott
	Southwest Indian Ridge					
-55.55	-0.15	-53.85	2.70	2	1	Bouvet
-54.35	4.45	-54.25	4.70	2	1	Moshesh
-54.55	5.55	-53.90	6.45	2	1	Islas
-54.30	7.95	-52.45	10.55	2	1	Shaka
-52.75	12.80	-52.00	13.75	2	1	Dingaan
-52.35	15.10	-52.10	15.50	2	1	
-52.22	16.08	-52.00	16.45	2	1	
-52.65	18.55	-52.45	18.75	2	1	
-52.70	19.65	-52.45	19.80	2	1	
-53.00	22.85	-52.80	23.00	2	1	
-53.35	25.30	-52.40	26.00	2	1	
-52.65	28.00	-47.50	32.00	2	1	
-47.60	33.00	-46.90	33.95	2	1	
-45.80	34.90	-45.35	35.20	2	1	Prince Edw
-44.30	39.10	-43.75	39.35	2	1	
-43.55	41.50	-42.50	41.75	2	1	Discovery
-42.40	42.45	-41.40	42.75	2	1	Discovery
-41.00	45.85	-38.85	46.25	2	1	Indomed
-38.65	47.90	-38.30	47.95	2	1	
-38.10	49.20	-37.85	49.25	2	1	
-37.25	52.25	-36.25	52.40	2	1	Gallieni
-36.00	53.30	-35.75	53.32	2	1	
-35.60	54.00	-34.80	54.15	2	1	
-34.60	54.85	-34.30	54.90	2	1	
-34.20	55.70	-33.90	55.75	2	1	
-33.80	56.45	-33.55	56.50	2	1	
-33.30	56.95	-32.80	57.00	2	1	Atlantis
-32.40	57.60	-31.80	57.70	2	1	
-31.65	58.40	-31.25	58.45	2	1	
-30.75	59.50	-30.25	59.52	2	1	
-29.75	60.70	-28.90	60.75	2	1	Melville

* L, Left and R, Right Plates: 1, African; 2, Antarctic; 3, Arabian; 4, Caribbean; 5, Cocos; 6, European; 7, Indian; 8, Nazca; 9, North American; 10, Pacific; 11, South American.

angle between the overall trend of the ridge and the spreading direction.

A plot of transform length versus ridge segment length is shown in Figure 3. The digitized ridges consist of 142 stepped patterns and 30 crenelate patterns. In Figure 3 the upper part of each vertical bar represents the offset of the northern transform, while the lower line represents the southern transform. Ridge segment lengths vary from 33 km to 1090 km and average 160 km in length. Transform offsets range between 0 km and 922 km and average about 120 km. Based on these data, there is little or no correlation between ridge segment length and transform length. There is also little or no correlation between spreading rate and transform length as shown in Figure 4. Figure 4 also shows there are many more slow (<30 mm/yr) slipping transform faults than fast slipping (>30mm/yr) ones. Note that the undigitized ridges are slow spreaders, so they will not contribute to this study.

There is a weak correlation between ridge segment length and the angle between the overall trend of the ridge and the spreading direction (see Figure 5). The angle Θ in Figure 5 is

$$\Theta = \tan^{-1}[2R/(O_1+O_2)] \quad (1)$$

where O_1 and O_2 are the lengths of the transform faults adjacent to each ridge segment R. If all transforms had the same offset, then there should be a perfect correlation between Θ and ridge segment length R. It is surprising the correlation is not better.

The unexpected poor correlation between ridge segment length and spreading angle occurs because ridge segment length correlates better with spreading rate, as shown in Figure 6. The slower spreading ridge segments (<20 mm/yr) are generally shorter than 200 km. This maximum length ridge increases with spreading rate to a value of 1090 km at 80 mm/yr. At all spreading rates there are ridge segments shorter than the maximum perhaps reflecting the influence of spreading angle.

To separate the effects of angle Θ and rate v on ridge segment length R, the following planar surface was fit to the data:

$$R = Av + B\Theta + C \quad (2)$$

The least squares fit of this model to the 169 ridge segment length data shows A = 6.28 $\pm$ 0.45 m.y., B = 1.67 $\pm$ 0.34 km/deg, and C = -74.2 $\pm$ 22.0 km. The slope parameters A and B alone reduce the variance of the residuals (with respect to the residuals about the mean) by 58%. (The Θ parameter was preferred over tan(Θ) because it resulted in a greater variance reduction.) The projection of the ridge segment length data back to zero spreading rate is shown in Figure 7*a*. Also shown is the model prediction (solid line). Ridge segment length increases by 150 km between 0° and 90°. The rms scatter of the data about this line is 91 km. The projection of the data to perpendicular spreading is shown in Figure 7*b*. The model (solid line) predicts that the ridge segment length increases by 502 km between 0 spreading rate and 80 mm/yr. The rms scatter about this line is also 91 km, and the scatter increases with increasing spreading

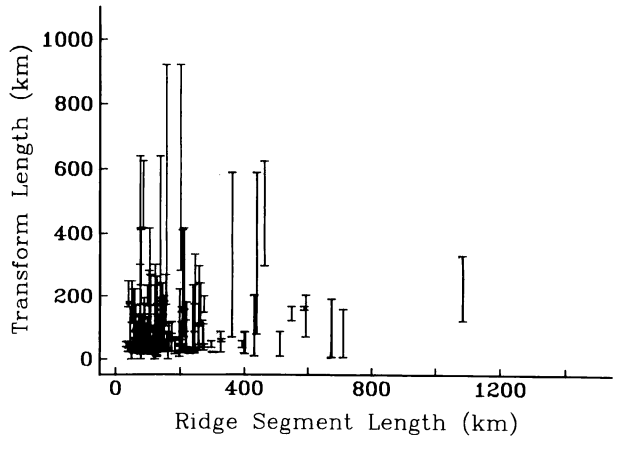

Fig. 3. Transform length versus ridge segment length. Upper and lower ends of bar represent transform lengths north and south of a ridge segment, respectively.

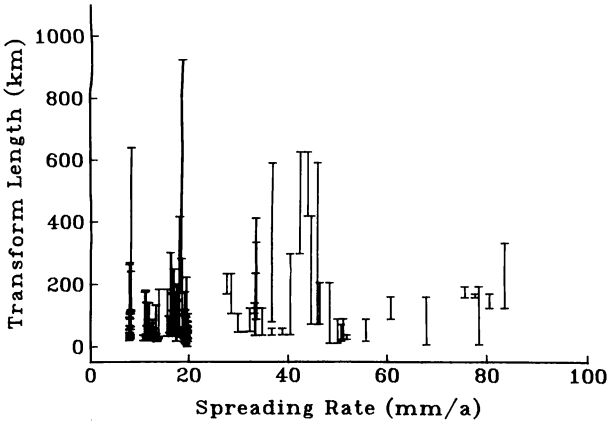

Fig. 4. Transform length versus spreading rate.

rate. This analysis indicates that ridge segment length depends primarily upon spreading rate and secondarily on spreading angle.

Lithospheric Strength Versus Age

The high correlation between ridge segment length and spreading rate can be explained by a thermoelastic model of the lithosphere similar to the one proposed by *Turcotte* [1974]. The rheology and geometry of the model are shown in Figures 8*a* and 8*b*, respectively. Mantle material upwelling at the spreading center is viscous and does not support shear stress over long periods of time (Figure 8*a*, left). This material freezes to the base of the lithosphere and continues to cool by heat conduction. For temperatures below T_l it can sustain shear stress on geologic time scales. Actually, the stress-strain relation for rock at temperatures below T_l is highly nonlinear [*Griggs et al.*, 1960] and is well approximated by an elastic-perfectly plastic rheology [*Turcotte et al.*, 1978], as shown in Figure 8*a* (middle). The yield stress σ_y of the lower part of the lithosphere decreases with increasing depth and temperature [*Goetze and Evans*, 1979]; this defines the lower part of the yield envelope.

Yielding of the upper lithosphere is controlled by brittle fracture. The stress-strain relation is linear until the fracture stress is attained (Figure 8*a*, right). According to Byerlee's law [*Byerlee*, 1978], compressional yielding occurs when one of the horizontal stress components is 3–5 times greater than the overburden pressure. The factor depends upon the magnitude of the lithostatic stress and the fluid pore pressure [*Brace and Kohlstedt*, 1980]. Tensional failure occurs at lower stresses of 0.2–0.3 times the overburden pressure. The lower lithosphere ductile yield criterion and the upper lithosphere brittle fracture criterion combine to produce the yield stress versus depth curve or the yield envelope. The overall strength of the lithosphere is the integral of yield stress over depth; it increases nearly linearly with increasing lithospheric age.

Thermoelastic Model

Thermal stress in the elastic part of the lithosphere results from nonuniform cooling and contraction. In a cooling elastic body, thermal stress is high in regions of rapidly varying temperature gradient (e.g., near the spreading ridge), and thermal stress is zero where temperature gradients are constant (e.g., old oceanic lithosphere) [*Boley and Weiner*, 1960]. At a given distance from the ridge the upper part of the lithosphere is in compression while the lower part is in tension. This depth-dependent stress produces a thermal bending moment M_T, causing the lithosphere to flex. Furthermore, if the plate is not allowed to shrink in the along-ridge direction, then thermal tensile stress will develop. The integral over depth of the thermal stress is the thermal end load N_T.

Let l be the depth to the T_l isotherm and $\Delta T(z) = T(z) - T_l$ be the local difference between the local temperature and the blocking temperature T_l. Then

$$N_T = -\int_0^l \alpha E \, \Delta T(z) \, dz \tag{3}$$

and

$$M_T = -\int_0^l \alpha E \, \Delta T(z) \, (z - 1/2) \, dz \tag{4}$$

where α is the linear expansion coefficient and E is Young's modulus [*Boley and Weiner*, 1960]. Parameter values are given in Table 2. It is shown below that large thermal stresses only occur in young oceanic lithosphere. Thus the cooling half-space temperature model is used

$$T(x,z) = T_o + (T_m - T_o) \ \mathrm{erf}[z/2 \ (v/\kappa x)^{1/2}] \tag{5}$$

The surface temperature is T_o, T_m is the mantle temperature, and κ is the thermal diffusivity. Equation (3) can be integrated for the temperature structure given in (5). The result is

$$N_T = -2\alpha E \, (T_m - T_o) \, [1 - \exp(-\delta^2)] \, (\kappa x/\pi v)^{1/2} \tag{6}$$

where $\delta = \mathrm{erf}^{-1}(T_l/T_m)$ is the fractional thickness of the competent part of the lithosphere. The thermal end load N_T is proportional to the square root of the age of the lithosphere. Unlike *Turcotte*'s [1974] analysis, it is assumed here that the product of αE does not change across the moho. This αE contrast enhances M_T through the bimetallic strip effect but has little effect on N_T.

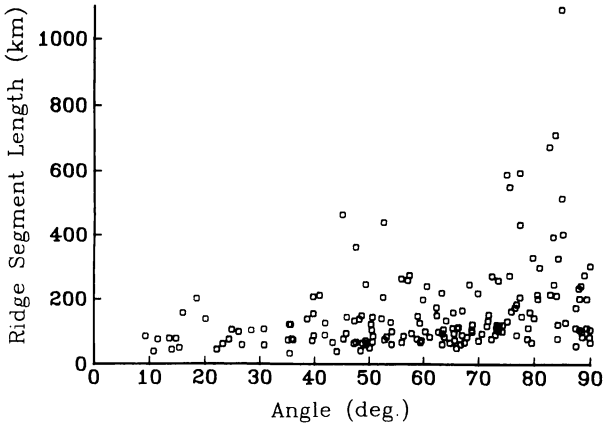

Fig. 5. Ridge segment length versus spreading angle. The angle is measured between the spreading direction and the line bisecting adjacent transforms (see Figure 1).

Since the elastic part of the lithosphere is thin compared with the scale of the lateral variations in temperature (except at the ridge), a plane stress approximation is used (i.e., $\sigma_{zz} = \sigma_{xz} = \sigma_{yz} = 0$). *Boley and Weiner* [1960] show that for thin plates the average of the temperature over depth times E (i.e., N_T) results in stresses in the x-y plane only. The first moment of the temperature with respect to depth times E (i.e., M_T), on the other hand, produces lithospheric flexure. The thickness of the elastic part of the lithosphere increases as the square root of age. To avoid mathematical complexity, this variable thickness elastic layer is approximated by a constant thickness layer. Because of this approximation, the model will overestimate stresses (i.e., stress integrated over the plate thickness) near the ridge and underestimate stresses in older lithosphere. The differential equation describing the in-plane stress is

$$\nabla^4 F = -\nabla^2 N_T \tag{7}$$

where F is the Airy stress function [*Boley and Weiner*, 1960]. The stress components integrated over depth are

$$N_y = \partial^2 F/\partial x^2 \quad N_{xy} = -\partial^2 F/\partial x \partial y \quad N_x = \partial^2 F/\partial y^2 \tag{8}$$

For lack of knowledge about the tractions at the boundaries of the plate, it is assumed all boundaries are traction free. The mathematical statement of this is $F = dF/dn = 0$, where n is the outward normal to the boundary. The material freezing onto the underside of the plate, near the ridge, begins with no shear stress. Therefore the appropriate ridge boundary condition is that all three components of stress should be zero.

Three solutions to (7) with increasingly complex boundary conditions are presented below. In the simplest model [*Turcotte*, 1974], the plate is infinite in the y direction and extends from zero to infinity in the x direction. The differential equation and boundary conditions simplify to

$$d^2F/dx^2 = -N_T \tag{9}$$

$$N_y(0) = 0 \tag{10}$$

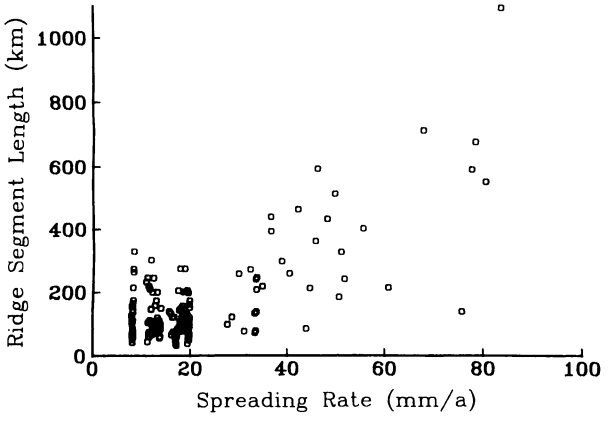

Fig. 6. Ridge segment length versus spreading rate.

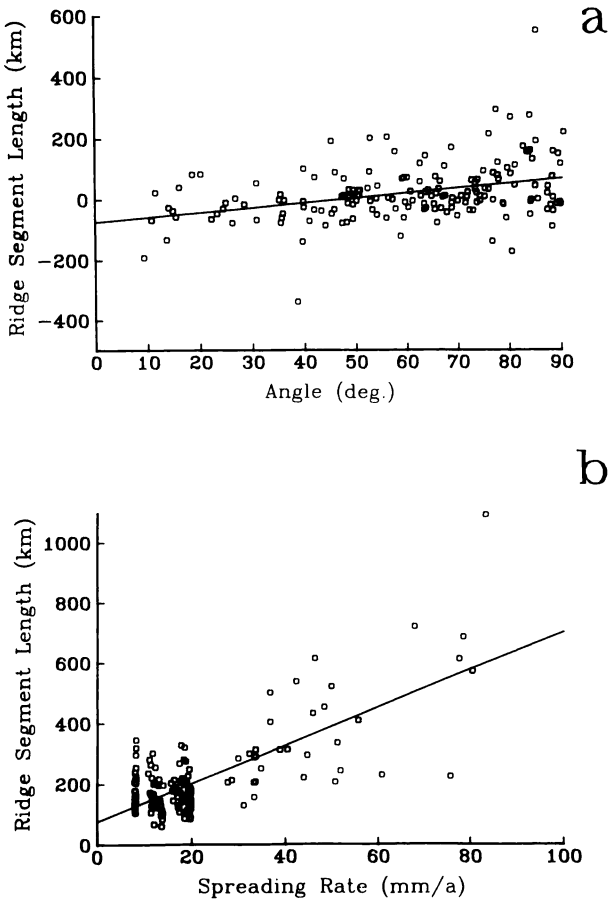

Fig. 7. *(a)* Ridge segment lengths versus spreading angle corrected to zero spreading rate. Solid line is best fitting plane. *(b)* Ridge segment length versus spreading rate corrected to orthogonal spreading. Solid line is best fitting plane.

The solution is

$$N_y(x) = 2\alpha E\,(T_m - T_o)[1 - \exp(-\delta^2)]\,(\kappa x/\pi v)^{1/2} \tag{11}$$

Tensile stress is parallel to the ridge and increases as the square root of distance from the ridge.

While this model is simple, it is unrealistic because oceanic plates have finite lengths and widths. If thermal stress is not transmitted across plate boundaries, then interior stress will be significantly lower than predicted by this model. The differential equation and boundary conditions for a plate that is infinite in the y direction and extends fron 0 to L in the x direction are

$$d^4F/dx^4 = -d^2N_T/dx^2 \tag{12}$$

$$d^2F/dx^2 = 0 \qquad x = 0 \tag{13}$$

$$dF/dx = 0 \qquad x = 0, L \tag{14}$$

the general solution to this problem is

$$N_y(x) = -N_T'(x) + 2x/L \int_0^L N_T'(\xi)\,d\xi \tag{15}$$

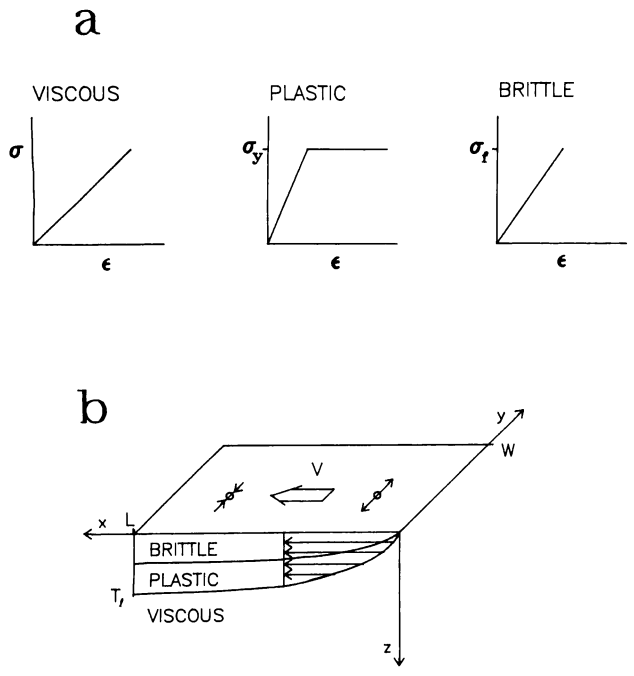

Fig. 8. *(a)* Hot mantle material is viscous, lower lithosphere is elastic-plastic and upper lithosphere is elastic-brittle. *(b)* Lithosphere is created at x=0 and spreads in x-direction at velocity v. The plate has finite length, L, and finite width w.

where

$$N_T'(x) = N_T(x) - N_T(0) \tag{16}$$

For the end load given in (6) the solution is

$$N_y(x) = 2\alpha E\,(T_m - T_o)[1 - \exp(-\delta^2)] \cdot(\kappa L/\pi v)^{1/2}\,[(x/L)^{1/2} - 4x/3L] \tag{17}$$

This solution has the same square root dependence as the previous solution; however, it also includes a term that decreases linearly with distance from the ridge. The plate is in tension near the ridge and goes into compression at a distance of 9/16 L from the ridge.

The stress versus age curves for these two solutions are shown in Figure 9. The infinitely long plate (solid curve) has higher stress than the finite length plate (dashed curve; L = 2000 km, v = 20 mm/yr). Also shown (dotted curve) is the tensile strength of the lithosphere versus age (described in previous section). Stress in the infinitely long plate exceeds the strength of the lithosphere for ages between 0 and 27 Ma. Such high stresses led *Turcotte* to propose that tensional failure occurs along transform faults. For the finite length plate stresses are significantly lower but still exceed the strength of the lithosphere between ages of 0 and 8 Ma. The stress versus age curve for the finite length plate depends upon the length of the plate and the spreading rate. As the length of the plate is increased and the spreading rate is decreased, this solution approaches the infinite length solution. Both solutions are physically unrealistic because they have tensile stresses which exceed the strength of the lihtosphere near the ridge.

To test *Turcotte*'s [1974] hypothesis that transform faults relieve thermal stress, the oceanic lithosphere is modelled as a rectangular strip (Figure 8*b*). The finite width W of the plate represents the segment of lithosphere lying between adjacent fracture zones. This approximates the expected low coupling of tensile stress across the active transform faults. Since the plates are bonded along the inactive portion of the fracture zone a more appropriate model would have either a stepped or crenelate traction free boundary. The strip approximation may not be too bad, however, because most of the thermal contraction occurs close to the ridge and close to a transform fault. For the stepped pattern, which dominates observed ridge-transform geometries, each strip is bounded by only one transform fault (see Figure 1) instead of two as implied by the model. A crude way of accounting for this discrepancy is to use twice the ratio of W/v in the model. The plate also has a finite length L as before. The smaller of the width and the length controls the level of stress in the plate interior. The differential equation and boundary conditions that must be solved are

$$\nabla^4 F = -\nabla^2 N_T \tag{18}$$

$$\partial^2 F/\partial x^2 = \partial^2 F/\partial x\partial y = 0 \qquad y = \pm W/2 \tag{19}$$

$$\partial^2 F/\partial y^2 = \partial^2 F/\partial x\partial y = 0 \qquad x = 0, L \tag{20}$$

$$\partial^2 F/\partial x^2 = 0 \qquad x = 0 \tag{21}$$

where N_T is given in (6). A similar problem is solved by *Timoshenko and Goodier* (1970, p. 439). The solution is outlined in the appendix.

TABLE 2. Definitions and Values of Parameters

Parameter	Definition	Value
α	linear expansion coefficient	10^{-5} °K^{-1}
E	Young's modulus	6.5×10^{10} Pa
κ	thermal diffusivity	8.0×10^{-7} m^2 s^{-1}
T_l	blocking temperaturee	740°C
T_m	mantle temperature	1356°C
T_o	surface temperature	0°C

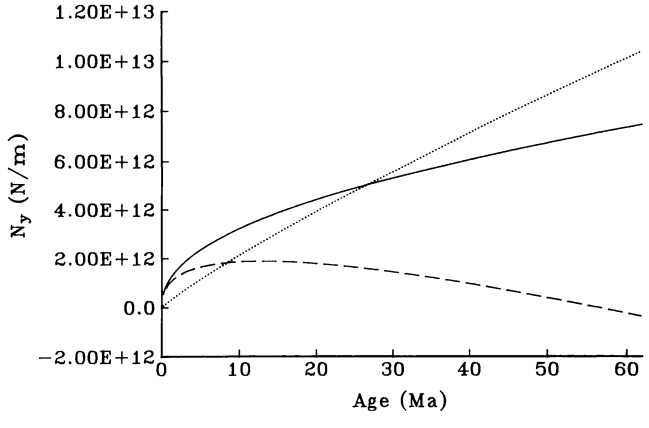

Fig. 9. Thermoelastic stress (positive-tension) for semi-infinite plate (solid curve) and finite length plate (dashed curve, L = 200 km, v = 20 mm/yr). The strength of the lithosphere in tension (dotted curve) is less than the thermal tensile stress in young lithosphere.

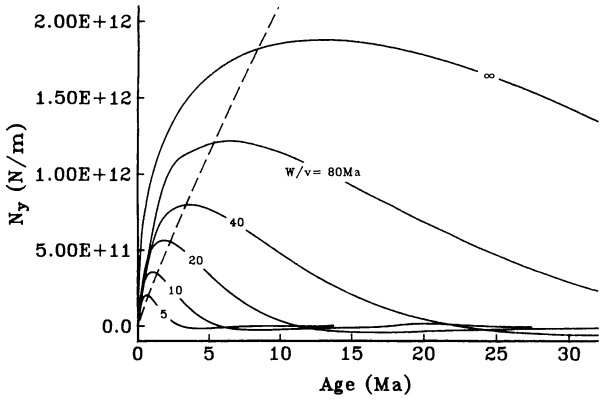

Fig. 10. Thermoelastic tensite stress for plate of finite length an widths (solid curves). Stress is governed by the ratio of width to spreading rate. Dashed curve is the strength of the lithosphere in tension.

The solutions for the three stress components, given in equations (A23) - (A25) of the appendix, reveal the linear relationship between the plate width and the wavelength of the temperature field $\lambda_n = 2\pi/k_n$. The magnitude of each stress compunent at $y = 0$ is a function of W/λ_n. When $W >> \lambda_n$ stresses are high. Stresses are low when $W << \lambda_n$. Before stresses can be calculated using equations (A23) - (A25), the temperature structure of the cooling half-space must be decomposed into a Fourier sine series; each coefficient a_n is computed from (A16). Suppose the Fourier coefficients were calculated for a spreading rate of v. If v is then doubled, then the coefficients a_n will have the same values as before but they will correspond to a wavelength of $2\lambda_n$ rather than λ_n. Since λ_n is proportional to v, the parameter determining the magnitude of the stress is W/v.

To calculate stresses for a cooling lithosphere, N_T was made into an odd continuous function to ensure imaginary Fourier coefficients. The y component of stress at $y = 0$ is plotted in Figure 10 for various ratios of plate width to spreading rate ranging from 5 to ∞ Ma. Near the ridge (i.e., age << W/v) the stress field is unaffected by the finite length and finite width of the plate so N_y increases as $(\text{age})^{1/2}$. The stress begins to level off and then decreases

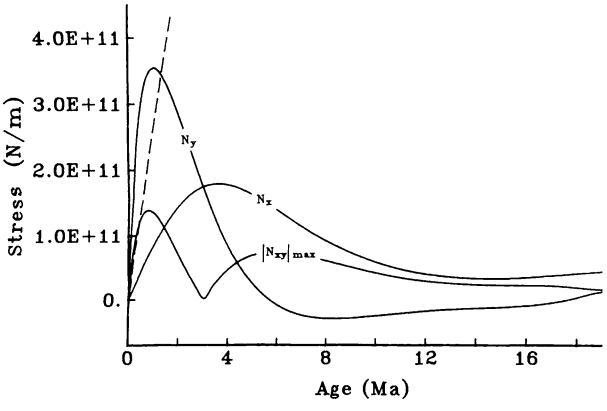

Fig. 11. Stress components at y = 0 for W/v = 10 m.y. (solid curves). Stresses are zero at the spreading ridge and mostly tensile between 0 and 10 Ma. All stress components are small for ages greater than 10 Ma.

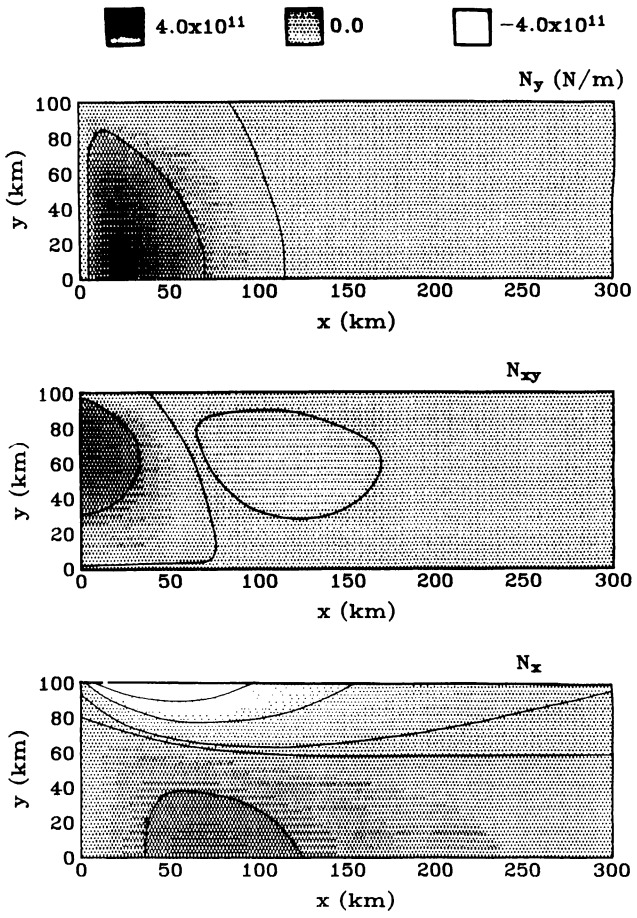

Fig. 12. Spatial patterns of thermoelastic stress components in cooling lithosphere W = 200 km, v = 20 mm/yr. Largest tensile stress occurs at $y = 0$, x = 25 km.

as the age approaches $W/2v$. The lithosphere is in compression for ages greater than $W/2v$. Also plotted (dashed curve) is the tensional strength of the lithosphere versus age. Thermal stresses exceed the strength of the lithosphere very near the ridge. The age where the stress falls below the strength increases with increasing W/v.

The observed ratio of ridge segment length to spreading rate is 6.28 Ma (see Figure 7*b*). To account approximately for the predominance of stepped, ridge-transform geometries, the model W/v ratio is increased to 10 m.y. Stress components (at $y = 0$) for this W/v ratio are shown in Figure 11. N_y is tensile between ages of 0 and 5 Ma and slightly compressional at greater ages. N_x is tensile at all ages but decreases markedly beyond 10 Ma. The maximum shear stress $|N_{xy}|_{max}$ (i.e., one half the difference between the two principal stresses) is also shown in Figure 11. For this value of W/v the thermal stress only exceeds the strength of the lithosphere between ages of 0 and 0.5 Ma. At greater ages all stress components are substantially lower than the strength of the lithosphere. Thus transform faults, with the observed ratio of spacing to spreading rate (i.e., 6.28 Ma), effectively relieve the thermal stress caused by cooling and contraction of the lithosphere.

The spatial patterns of the three stress components are shown in Figure 12 for W/v = 10 m.y. (i.e., W = 200 km, v = 20 mm/yr). The y component of stress (upper) is tensile near the ridge and goes to zero at $y = \pm 100$ km. The shear stress (middle) is zero at y = 0 and at y = ±100 km. The

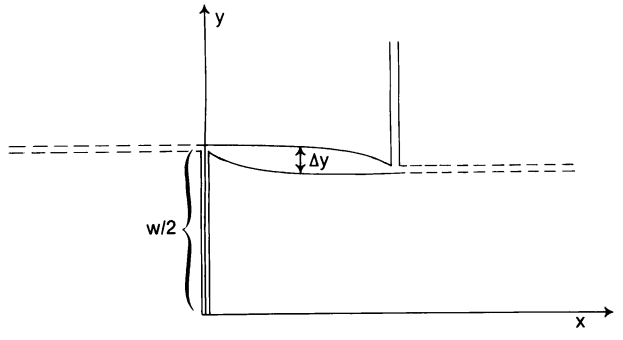

Fig. 13. Shrinkage of the lithosphere away from the ridge results in a wide depression along transform fault and fracture zone (modified from *Collette*, 1974).

nonzero shear stress at the ridge violates the desired zero traction boundary condition. The x component of stress is tensile over most of the plate interior except near the transform boundaries where it is highly compressive. While the boundary stresses predicted by this model do not agree with expected tractions along ridge and transform boundaries [*Lachenbruch*, 1973; *Morgan and Parmentier*, 1984], the internal stresses are qualitatively correct and explain the observed relationship between ridge segment length and spreading rate.

Discussion

The thermoelastic model predicts stress and strain for a cooling strip of lithosphere. If the model is valid, then the predictions must agree with other geophysical observations. It must also explain the development of the orthogonal ridge and transform pattern in the wax spreading models [*Oldenburg and Brune*, 1972].

One model prediction is that crustal fractures should develop in the first one million years because thermal stress exceeds lithospheric strength. Models of hydrothermal circulation [*Lister*, 1972; *Sleep and Wolery* 1978] indicate that fractures extend several kilometers into the young lithosphere. These fractures not only relieve thermal stress but they also allow water to circulate, cool, and strengthen the lithosphere. Hydrofracturing at the ridge may also be responsible for some of the earthquakes there.

For ages greater than 1 Ma the earthquake frequency decreases substantially [*Wiens and Stein*, 1983, 1984; *Bergman and Solomon*, 1984]. Off-ridge earthquakes occuring in 1 - 35 m.y.-old lithosphere are primarily normal events with tensional axes parallel to the ridge. Both groups studying these earthquakes proposed that they were caused by thermal stress. Their observations reinforce the thermoelastic model which predicts that tensile stress is aligned with the ridge and all thermal stress components decrease rapidly with age.

Recently, *Bratt et al.* [1985] modelled thermal stress in the cooling lithosphere. In most respects their model was similar to the model in this study, although they used an elastic half-space rather than a thin elastic plate. To relieve stress as the lithosphere ages, they incorporated a characteristic stress relaxation time. This relaxation occurs by brittle fracture of the upper lithosphere and ductile flow of the lower lithosphere. Their model correctly predicts the observed age distribution and type of earthquakes. Good agreements, however, depend upon using a relaxation time that is substantially shorter than has been observed in laboratory experiments [*Goetze and Evans*, 1979]. It is shown here that stress relaxation is unnecessary because transform faults relieve thermal stress. The characteristic stress release time is governed by the ratio of ridge segment length to spreading rate. One means of discriminating between the two models is to see if there is a correlation between earthquake frequency and the ratio of W to v as predicted by the model developed here.

A second model prediction is that the stress relief at transform faults allows the lithosphere to shrink almost freely in the direction parallel to the ridge [*Collette*, 1974]. Equal unimpeded shrinkage in all three dimensions is assumed in the depth versus age models incorporating the volume coefficient of thermal expansion [*McKenzie*, 1967; *Davis and Lister*, 1974]. *Collette* [1974] first noted that the y direction shrinkage is responsible for the deep valleys along transform faults. The amplitude of the free contraction in the y direction at a given depth is

$$\Delta y(x,z) = -\alpha W/2\ [T_l - T(x,z)] \qquad (22)$$

The volume of contracted material per unit length along the transform is the integral of (22) over depth and is

$$V(x) = -\alpha W\ (T_m - T_o)[1 - \exp(-\delta^2)]\ (\kappa x/\pi v)^{1/2} \qquad (23)$$

Figure 13 is a diagram of the basin that develops along the transform fault and its continuation out onto the fracture zones. The maximum volume of missing lithosphere should occur half way between the two ridges and should have an amplitude proportional to the square root of the age offset. If the width and shape of transform valleys were known, then the model could be used to determine if the crack is being filled in from below with hot mantle material.

Finally, the thermoelastic model should be reconciled with the wax spreading experiments of *Oldenburg and Brune* [1972, 1975]. It is unlikely that different physical mechanisms are responsible for the orthogonal ridge and transform patterns in the wax and in the oceanic lithosphere. *Oldenburg and Brune* [1972] found that the

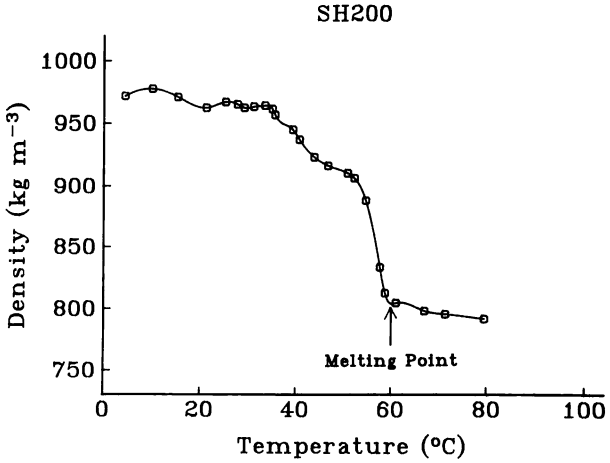

Fig. 14. Thermal expansion curve for Shell wax 200 which supported orthogonal ridge-transform pattern in the wax spreading experiments.

orthogonal pattern was easier to develop and maintain in waxes with high shear strength and tensile strength. Moreover, the pattern only existed for a certain range of spreading rates. If transform faults exist primarily to relieve thermal stress, then thermal stress must also be high in waxes displaying the orthogonal ridge and transform pattern. The temperature difference between the hot solidified wax and the upper surface of the solid wax was perhaps only 10°C in the experiments. Shell wax 200, in which the orthogonal pattern develops easily, changes density by more than 10% over a 10°C temperature range just below the melting point as shown in Figure 14 (R. Dannenbrink, personal communication, Shell Oil Company, Houston, Texas, 1985). This indicates that unusually high thermal stresses exist in cooling Shell wax 200. Based on these wax expansion data, it appears that both the lithospheric transform faults and the wax transform faults exist to relieve thermal stress.

APPENDIX

The Airy stress function is divided into a particular solution F^P and a complementary solution F^C. The particular solution satisifies (18) but not the boundary conditions, (19)—(21). It is

$$F^P = 4/15\ \beta x^{5/2} \tag{A1}$$

where

$$\beta = 2\alpha E\ (T_m - T_0)\ [1 - \exp(-\delta^2)]\ (\kappa/\pi v)] \tag{A2}$$

The mismatch of this solution to boundary condition (19) at $y = \pm W/2$ is resolved by the complementary solution with the negative of the boundary values. This reduces the thermoelastic problem to a constant temperature elasticity problem but with a different boundary condition

$$\nabla^4 F^C = 0 \tag{A3}$$

$$\partial^2 F^C/\partial x^2 = -\beta x^{1/2},\quad y = \pm\Omega \tag{A4}$$

$$\partial^2 F^C/\partial x \partial y = 0,\quad y = \pm\Omega,\ x = 0,\ L \tag{A5}$$

$$\partial^2 F^C/\partial y^2 = 0,\quad x = 0,\ L \tag{A6}$$

$$\partial^2 F^C/\partial x^2 = 0,\quad x = 0 \tag{A7}$$

where $\Omega = W/2$.

It is assumed that F^C can be decomposed as follows:

$$F^C(x,y) = \sum_{n=-\infty}^{\infty} \phi_n(y) \exp(ik_n x) \tag{A8}$$

where $k_n = 2\pi n/L$. The functions $\phi_n(y)$ must be determined from the differential equation and the boundary conditions. Inserting (A8) into (A3) results in the following fourth-order, ordinary differential equation:

$$d^4\phi_n/dy^4 - 2k_n^2\ d^2\phi_n/dy^2 + k_n^4\ \phi_n = 0 \tag{A9}$$

The general solution is

$$\phi_n(y) = A_n \exp(k_n y) + B_n \exp(-k_n y) + C_n k_n y\ \exp(k_n y) - D_n k_n y\ \exp(-k_n y) \tag{A10}$$

The solution must be symmetric about $y = 0$, so

$$A_n = B_n \quad C_n = D_n \tag{A11}$$

The complementary solution is

$$F^C = \sum_{n=-\infty}^{\infty} \exp(ik_n x)\ [A_n \cosh(k_n y) + C_n\ k_n y\ \sinh(k_n y)] \tag{A12}$$

where A_n and C_n were multiplied by two. The coefficients A_n and C_n are determined from the boundary conditions (A4) and (A5). Consider boundary condition (A5) at $y = \Omega$

$$\partial^2 F^C/\partial x \partial y = 0 = \sum_{n=-\infty}^{\infty} ik_n^2 \exp(ik_n x)\{A_n \sin(k_n\Omega) + C_n[\sinh(k_n\Omega) + k_n\Omega \cosh(k_n\Omega)]\} \tag{A13}$$

Each term in the series must vanish so

$$A_n = -C_n\ [\sinh(k_n\Omega) + k_n\Omega \cosh(k_n\Omega)] \cdot [\sinh(k_n\Omega)]^{-1} \tag{A14}$$

The boundary (A4) is used to determine C_n, but first (A4) must be expanded in a Fourier series.

$$\partial^2 F^C/\partial x^2 = \sum_{n=-\infty}^{\infty} a_n \exp(ik_n x) \qquad y = \pm\Omega \tag{A15}$$

The coefficients a_n are

$$a_n = -1/L \int_0^L \beta x^{1/2} \exp(-ik_n x)\ dx \tag{A16}$$

The second derivative of F^C with respect to x evaluated at Ω is

$$\partial^2 F^C/\partial x^2 = -\sum_{n=-\infty}^{\infty} k_n^2 \exp(ik_n x)\ [A_n \cosh(k_n\Omega) + C_n k_n \Omega\ \sinh(k_n\Omega)] \tag{A17}$$

Individual terms in (A15) and (A17) must be equal

$$a_n = -k_n^2\ [A_n \cosh(k_n\Omega) + C_n k_n W \sinh(k_n\Omega)] \tag{A18}$$

After inserting (A14) into (A18) and rearranging terms one obtains

$$C_n = 2a_n k_n^{-2} \sinh(k_n\Omega)[\sinh(2k_n\Omega) + 2k_n\Omega]^{-1} \tag{A19}$$

The coefficients A_n are determined by inserting (A19) into (A14). They are

$$A_n = -2\ a_n k_n^{-2}[k_n\Omega \cosh(k_n\Omega) + \sinh(k_n\Omega)] \cdot [\sinh(2k_n\Omega) + 2k_n\Omega]^{-1} \tag{A20}$$

The final solution is

$$F^C = \sum_{n=-\infty}^{\infty} -2a_n k_n^{-2}\, g_n(\Omega)\exp(ik_n x) \cdot\{[k_n\Omega\cosh(k_n\Omega) + \sinh(k_n\Omega)]\cosh(k_n y) - \sinh(k_n\Omega)\, k_n y \sinh(k_n y)\} \quad \text{(A21)}$$

where

$$g_n(\Omega) = [\sinh(2k_n\Omega) + 2k_n\Omega]^{-1} \quad \text{(A22)}$$

and $\Omega = W/2$.

The three stress components, found by differentiating (A21) are

$$N_x = \sum_{n=-\infty}^{\infty} -2a_n\, g_n(\Omega)\exp(ik_n x) \cdot\{[k_n\Omega\cosh(k_n\Omega) - \sinh(k_n\Omega)]\cosh(k_n y) - \sinh(k_n\Omega)\, k_n y \sinh(k_n y)\} \quad \text{(A23)}$$

$$N_y = \sum_{n=-\infty}^{\infty} 2a_n\, g_n(\Omega)\exp(ik_n x) \cdot\{[k_n\Omega\cosh(k_n\Omega) + \sinh(k_n\Omega)]\cosh(k_n y) - \sinh(k_n\Omega)\, k_n y \sinh(k_n y)\} \quad \text{(A24)}$$

$$N_{xy} = \sum_{n=-\infty}^{\infty} 2ia_n\, g_n(\Omega)\exp(ik_n x)\,[k_n\Omega\cosh(k_n\Omega)\sinh(k_n y) - \sinh(k_n\Omega)\, k_n y\cosh(k_n y)] \quad \text{(A25)}$$

For an arbitrary temperature structure, the boundary conditions at $x = 0$ and $x = L$ can only be approximately matched. Suppose that a_n is imaginary (i.e., N_T can be expanded in a Fourier sine series), then N_x and N_y are zero at $x = 0$, but N_{xy} is not. Even though this solution does not exactly match the boundary conditions, it correctly shows the effect of the finite plate width.

Acknowledgments. I thank Dallas Abbott for providing a preprint of her paper on ridge segmentation and Robert Dannenbrink for supplying the data on Shell Wax 200. I also thank the reviewers for their constructive comments. This work was supported by both the National Geodetic Survey and the University of Texas at Austin.

REFERENCES

Atwater, T., and K. C. Macdonald,, Are spreading centers perpendicular to thier transform failts?, *Nature*, *270*, 715-719, 1977.

Atwater, T., and H. W. Menard, Magnetic lineations in the northeast Pacific, *Earth Planet Sci. Lett.*, *7*, 445-450, 1970.

Bergman, E. A., and S. C. Solomon, Source mechanisms of earthquakes near mid-ocean ridges from body waveform inversion: Implications for the early evolution of oceanic lithosphere, *J. Geophys. Res.*, 89, 11415-11441, 1984.

Boley, B. A., and J. W. Weiner, *Theory of Thermal Stress*, pp. 379-409, John Wiley, New York, 1960.

Brace, W. K., and D. L. Kohlstedt, Limits on lithosphere stress imposed by laboratory experiments, *J. Geophys. Res.*, *85*, 6248-6252, 1980.

Bratt, S. R., E. A. Bergman, and S. C. Solomon, Thermoelastic stress: How important as a cause of earthquakes in young oceanic lithosphere? *J. Geophys. Res.*, *90*, 10249-10260, 1985.

Byerlee, J. D., Friction in rocks, *Pure Appl. Geophys .*, *116*, p. 615, 1978.

Canadian Hydrographic Service, General bathymetric chart of the oceans (GEBCO), 5th ed., Ottawa, Ont., 1982.

Chase, T. E., H. W. Menard, and J. Mammerickx, Bathymetry of the North Pacific, Insti. of Mar. Res., La Jolla, Calif., 1970.

Collette, B. J., Thermal contraction joints in spreading seafloor as origin of fracture zones, *Nature*, *251*, 299-300, 1979.

Crough, S. T., Geoid anomalies across fracture zones and the thickness of the lithosphere, *Earth Planet. Sci. Lett .*, *44*, 224-230, 1979.

Davis, E. E., and C. R. B. Lister, Fundamentals of ridge crest topography, *Earth Planet. Sci. Lett.*, *21*, 405-413, 1974.

Detrick, R. S., Jr., An analysis of geoid anomalies across the Mendocino Fracture Zone: Implications for thermal models of the lithosphere, *J. Geophys. Res.*, *86*, 11715-11762, 1981.

Dick, H. J. B., H. Schouten, and J. A. Whitehead, The wavelength selection mechanism below ridges, *EOS Trans. AGU*, *65*, 1088, 1984.

Fox, P. J., and D. G. Gallo, A tectonic model for ridge-transform-ridge plate boundaries: Implications for the structure of the oceanic lithosphere, *Tectonophysics*, *104*, 205-242, 1984.

Froidevaux, C., Energy dissipation and geometric structure at spreading plate boundaries, *Earth Planet. Sci. Lett.*, *30*, 419-424, 1973.

Goetze, R., and B. Evans, Stress and temperature in the bending lithosphere as constrained by experimental rock mechanics, *Geophys. J. R. Astron. Soc.*, *59*, 463-478, 1979.

Griggs, D. T., F. J. Turner, and H. C. Heard, Deformation of rocks at 500°C to 800°C, *Geol. Soc. Amer. Mem.*, *79*, 39-104, 1960.

Haxby, W. F., and D. L. Turcotte, On isostatic geoid anomalies, *J. Geophys. Res.*, *83*, 5473-5478, 1978.

Lachenbruch, A. H., A simple mechanical model for oceanic spreading centers, *J. Geophys. Res.*, *78*, 3395-3417, 1973.

Lister, C. R. B., On the thermal balance of a mid-ocean ridge, Geophys. *J. R. Astron. Soc.*, *26*, 515-535, 1972.

McKenzie, D. P., Some remarks on heat flow and gravity anomalies, *J. Geophys. Res.*, *72*, 6261-6273, 1967.

Menard, H. W., Evolution of ridges by asymmetrical spreading, *Geology*, *12*, 177-180, 1984.

Minster, J. B., and T. H. Jordan, Present-day plate motions, *J. Geophys. Res.*, *83*, 5331-5354, 1978.

Morgan, J. P., and E. M. Parmentier, Lithospheric stress near a ridge -transform intersection, *Geophys. Res. Lett.*, *11*, 113-116, 1984.

Oldenburg, D. W., and J. N. Brune, Ridge transform fault spreading pattern in freezing wax, *Science*, *178*, 301-304, 1972.

Oldenburg, D. W. and J. N. Brune, An explanation for the orthogonality of ocean ridges and transform faults, *J. Geophys. Res.*, *80*, 2575-2585, 1975.

Parsons, B., and J. G. Sclater, An analysis of the variation of ocean floor bathymetry and heat flow with age, *J. Geophys. Res.*, *82*, 803-827, 1977.

Sandwell, D. T., Along-track deflection of the vertical from Seasat: GEBCO overlays, NOAA Tech. Memo., NOS NGS-40, 1984.

Schouten, H., and K. D. Klitgord, The memory of the accreting plate boundary and the continuity of fracture zones, *Earth Planet Sci. Lett.*, *59*, 255-266, 1982.

Schouten, H., and R. S. White, Zero-offset fracture zones, *Geology*, *8*, 175-179, 1980.

Sleep, N. H., and T. J. Wolery, Egress of hot water from midocean ridge hydrothermal systems: Some thermal constraints, *J. Geophys. Res.*, *83*, 5913-5922, 1978.

Stein, S., A model for the relation between spreading rate and oblique spreading, *Earth Planet. Sci. Lett.*, *39*, 313-318, 1978.

Timoshenko, S. P., and J. N. Goodier, *Theory of Elasticity* , McGraw-Hill , New York, 1970.

Turcotte, D. L., Are transform faults thermal contraction cracks?, *J. Geophys Res.*, *79*, 2573-2577, 1974.

Turcotte, D. L., D. C. McAdoo, and J. G. Caldwell, An elastic-perfectly plastic analysis of the bending of the lithosphere at a trench, *Tectonophysics*, *47*, 193-205, 1978.

Vogt, P. R., and N. Z. Cherkis, Project i nvestigator I: Evolution of the Australia-Antarctic discordance deduced from a detailed aeromagnetic study, *Antarctic Earth Science*, pp. 608-613, 1983.

Wiens, D. A., and S. Stein, Age dependence of oceanic intraplate seismicity and implication for lithospheric evolution, *J. Geophys. Res.*, *88*, 6455- 6468, 1983.

Wiens, D. A., and S. Stein, Intraplate seismicity and stresses in young oceanic lithosphere, *J. Geophys. Res.* , *89*, 11442-11469, 1984.

Wilson, J. T., A new class of faults and their bearing on continental drift, *Nature*, *207*, 343-347, 1965.

Winterer, E. L., Anomalies in the tectonic evolution of the Pacific, in *The geophysics of the Pacific Ocean basin and its marg* in, *Geophys. Monogr. Ser.*, vol. 19, edited by, G. H. Sutton, M. H. Manghnani, and R. Moberly, pp. 269-280, AGU, Washington, D. C. , 1976.

D. T. Sandwell, Institute for Geophysics, University of Texas at Austin, 4920 North I. H. 35, Austin, TX 78712.

(Recieved June 10, 1985;
revised November 18, 1985;
accepted December 9, 1985.)